Atmospherically Forced and Chaotic Interannual Variability of Regional Sea Level and Its Components Over 1993–2015

Alice Carret, W. Llovel, Thierry Penduff, Jean-marc Molines

Correspondence to:
A. Carret,
alice.carret@legos.obs-mip.fr

Atmospherically Forced and Chaotic Interannual Variability of Regional Sea Level and Its Components Over 1993–2015

Alice Carret[1] , William Llovel[2] , Thierry Penduff[3] , and Jean-Marc Molines[3]

[1]Laboratoire d'Etudes en Géophysique et Océanographie Spatiale (LEGOS), CNRS/IRD/UPS/CNES, Toulouse, France, [2]Laboratoire d'Océanographie Physique et Spatiale (LOPS), University of Brest/IFREMER/IRD/CNRS, Brest, France, [3]Université Grenoble Alpes, CNRS, IRD, Grenoble-INP, Institut des Géosciences de l'Environnement (IGE), Grenoble, France

Abstract Satellite altimetry data have revealed a global mean sea level rise of 3.1 mm/yr since 1993 with large regional sea level variability. These remote data highlight complex structures especially in strongly eddying regions. A recent study showed that over 38% of the global ocean area, the chaotic variability may hinder the attribution to the atmospheric forcing of regional sea level trends from 1993 to 2015. This study aims to complement this work by focusing on the atmospherically forced and chaotic interannual variability of regional sea level and its components. At interannual time scales, variability can hamper the detection of regional sea level trends. A global 1/4° ocean/sea-ice 50-member ensemble simulation is analyzed to disentangle the imprints of the atmospheric forcing and of the chaotic ocean variability on the interannual variability of regional sea level and of its steric and manometric components over 1993–2015. The atmospherically forced and chaotic interannual variabilities of sea level mainly have a steric origin, except in coastal areas. The chaotic part of the interannual variability of sea level and its components is stronger in the Pacific and Atlantic Oceans than in the Indian Ocean. The chaotic part of the interannual variance of sea level and of its steric component exceeds 20% over 48% of the global ocean area; this fractional area reduces to 26% for the manometric component. These results confirm the substantial imprint of the chaotic interannual variability on sea level components, questioning in several regions the attribution of their observed evolution to atmospheric causes.

Plain Language Summary Since the early 1990s, satellite altimetry has become the main observing system for continuously measuring the sea level variations with a near global coverage. It has revealed a global mean sea level rise of 3.1 mm/yr since 1993 with large regional sea level variability that differs from the mean estimate. These measurements highlight complex structures especially for the western boundary currents (Gulf Stream or Kuroshio) or the Antarctic Circumpolar Current. Recent studies based on numerical modeling showed that the ocean spontaneously generates a chaotic intrinsic variability that substantially impacts the sea level interannual-to-decadal variability and its long-term trends. It is important to note that sea level observations simultaneously record these chaotic variations in the ocean but also the response to the atmospheric forcings. Here, we use a 50-member ensemble ocean simulation to disentangle the atmospherically forced and chaotic parts of the interannual variability of sea level and of its steric and manometric components. We found that, in several regions, the chaotic interannual variability has a large imprint on sea level components. While these results do not question the anthropic origin of global mean sea level rise, they give new insights into the oceanic vs. nonoceanic origin of regional interannual variability.

1. Introduction

Sea level change is one of the clearest consequences of the ongoing global warming. Thus, sea level has been identified as one of the Essential Climate Variables (ECVs) to monitor global warming, according to the Global Climate Observing System (GCOS). Global mean sea level (GMSL) rise is caused by an increase in Ocean Heat Content (OHC) which results in global mean thermal expansion (thermosteric sea level rise), and by the increase of freshwater content coming from continental ice melt (mountain glaciers melting and ice sheet mass loss from Greenland and Antarctica, Stammer et al., 2013).

Tide gauges have measured sea level along the coasts since the beginning of the 20th century, indicating a GMSL rise of 1.7 ± 0.4 mm/yr (Church et al., 2013). However, tide gauges only inform about sea level change at the coast with a hemispheric bias due to a larger number of stations located in the northern hemisphere (mainly European and American coasts). Since 1992, satellite altimetry observations have enabled a near global coverage with high accuracy to investigate sea level change. Satellite altimetry showed a GMSL rise of 3.1 ± 0.3 mm/yr (WCRP Global Sea Level Budget Group, 2018) over 1993–2017 that significantly differs from the tide gauge estimate over the 20th century, denoting a possible acceleration. A significant acceleration of 0.084 ± 0.025 mm/yr 2 of the altimetry-based GMSL rise has indeed been highlighted since 1993 (Nerem et al., 2018). While global mean sea level appears to be a good indicator of global warming, regional changes are most relevant for social and economic impact studies since 10% of the world's population is living near the coastlines at <10 m above sea level (Neumann et al., 2015).

At regional scales, other processes are at play. In addition to the drivers of GMSL changes, regional sea level variations are caused by changes in ocean circulation, wind stress, ocean-atmosphere heat and freshwater fluxes, regional ocean temperature and salinity changes, and geometric deformations of the sea floor (Bamber & Dawson, 2020; Church et al., 2013). For the first time, satellite altimetry has clearly highlighted the existence of spatial patterns in regional sea level trends with regions experiencing a sea level rise three times larger than the global estimate (Cazenave & Llovel, 2010). Therefore, the use of satellite altimetry enabled great advances by offering a synoptic view, a regular temporal sampling, and a free access to data in comparison to the unevenly distributed network of tide gauges (PSMSL, 2018). Therefore, satellite altimetry data helped improve our knowledge on sea level variations from global to regional scales.

Since the beginning of the 2000s with the launch of the Argo international program we have had access to an unprecedented amount of temperature and salinity in situ data from the surface to 2,000-m depth. These in situ profiles enable us to investigate the steric part (i.e., baroclinic effects) of the regional sea level changes deduced from satellite altimetry. In addition, the GRACE gravimetry mission launched in August 2002 enables us to estimate the mass component of sea level known as barystatic sea level at global scale and manometric sea level at regional scale (Gregory et al., 2019), associated with barotropic effects. The steric sea level derived from Argo can be combined with the barystatic/manometric sea level derived from GRACE since 2005 to study the sea level budget at global and regional scales. The steric and barystatic sea level components explain, respectively, 40% and 60% of it over 2005–2015 (Llovel et al., 2019), within the bounds of error of each measurement system (Willis et al., 2008).

It is also now well established that regional sea level trends inferred from satellite altimetry are in large part explained by thermosteric effects (Cazenave & Llovel, 2010) but at regional scales the halosteric part may be important (Llovel & Lee, 2015). However, some disagreements have yet to be understood: the regional sea level budget is not totally closed due to uncertainties in trends, errors in measurements or models, and poor sampling in some regions. The contributions (steric and manometric components) of the sea level trend budget vary from one region to another: the sea level trend reaches 14.7 mm/yr over 2002–2014 near the Philippines mostly due to the steric component of sea level whereas the manometric component of sea level dominates in the coastal North-eastern America (Rietbroek et al., 2016).

The drivers of regional sea level variability are, however, not only external to the ocean: eddy-permitting global ocean simulations (e.g., Llovel et al., 2018; Penduff et al., 2011, 2019; Sérazin et al., 2015) have demonstrated that the ocean spontaneously generates a chaotic intrinsic variability that substantially impacts the sea level interannual-to-decadal variability and its long-term trends. Indeed, spatial and temporal inverse cascades spontaneously transfer kinetic energy from the mesoscale to larger spatiotemporal scales (Arbic et al., 2014); these nonlinear processes are likely to feed part of the chaotic regional sea level low-frequency variability (Sérazin et al., 2018), as well as its trends over decadal to multidecadal time scales (Sérazin et al., 2016).

Llovel et al. (2018) further showed that over 38% of the global ocean area, this low-frequency chaotic variability may hinder the attribution to the atmospheric forcing of regional sea level trends computed over 1993–2015. Penduff et al. (2019) extended these investigations along the coasts of the global ocean and obtained a fractional area of 17%–20%.

Sea level change studies must therefore take into account the impacts of the atmospheric variability along with the chaotic ocean fluctuations to account for the full range of possible drivers, in particular within and in the vicinity of eddy-active regions. It is also mandatory to disentangle both contributions to identify the actual impact of the atmospheric variability on observed sea level components by observational records.

Forget and Ponte (2015) investigated the decomposition of the regional sea level interannual variability into an atmospherically forced contribution and a chaotic contribution. They assumed that atmospheric fluctuations mostly impact scales greater than 3° × 3° and that the remaining signal (below 3° × 3°) corresponds to the chaotic ocean variability. However, Close et al. (2020) have recently showed that the forced sea level variability does have a substantial imprint at these relatively small scales: one may thus question the validity of the assumption made by Forget and Ponte (2015).

In this study, we use a 50-member ensemble ocean simulation to disentangle the atmospherically forced and chaotic parts of the interannual variability of sea level and of its components. More precisely, we address the following questions:

- How much do the chaotic ocean variability and the atmospherically forced variability account for the interannual variability of regional sea level over 1993–2015?
- How much do these two types of variability impact the steric and manometric components of regional sea level?
- Do the different oceanic basins respond in the same way to the chaotic and atmospherically forced sea level interannual variability?

The paper is articulated as followed: Section 2 describes the data sets and the considered methodology to answer the scientific questions we raised. Section 3 assesses the model and Section 4 presents the main results of our study. Finally, Section 5 summarizes our results, addresses the implications of the findings, and discusses the future work motivated by this study.

2. Data and Methodology

2.1. The OCCIPUT Ensemble Simulation

The OCCIPUT (OceaniC Chaos: ImPacts, strUcture, predicTability) global ocean/sea-ice ensemble simulation is composed of 50 members integrated over the period 1960–2015. The numerical configuration is based on the version 3.5 of the NEMO model (Madec, 2008), with a horizontal resolution of 1/4° (27 km at the equator) and 75 geopotential levels; details about the model setup (subgrid-scale parameterizations, numerical schemes, etc.) are given in Bessières et al. (2017).

The 50 members were started on January 1, 1960 from a common 21-year spin-up. A small stochastic perturbation is applied in the equation of state (as in Brankart, 2013) within each member during 1960, then switched off during the rest of the simulation; this method generates an ensemble spread which grows and saturates after a few months up to a few years depending on the region. The 50 members are driven through bulk formulae during the whole 1960–2015 simulation by the same realistic 6-hourly atmospheric forcing (Drakkar Forcing Set DFS5.2, Dussin et al., 2016) derived from atmospheric reanalyzes.

In this study, we focus on the altimetric period (1993–2015); we make use of monthly averaged simulated sea level fields, and of its steric and manometric components recomputed from the three-dimensional model outputs.

2.2. Satellite Altimetry Data: The CCI Product

The CCI (Climate Change Initiative) project, setup by the European Space Agency, aims to obtain improved time series of ECVs, including sea level (Quartly et al., 2017). The data are corrected to suit climate studies (Legeais et al., 2018). We make use of the CCI sea level product, which combines all available satellite altimetry missions: ERS-1/2, GeoSat Follow-On, Envisat, TOPEX/Poseidon, Jason missions, SARAL/AltiKa, and CryoSat-2. All processing steps are applied to match the GCOS requirements, in particular, for the computation of sea level error budgets, or the monitoring of coastal regions.

The specific treatment and geophysical corrections applied to each mission are described in Ablain et al. (2017) and Quartly et al. (2017). The gridding process follows the SSALTO/DUACS System as described in Ablain et al. (2017). The resulting product has a near global coverage at 1/4° spatial resolution over the period 1993–2015 with a monthly temporal resolution.

Legeais et al. (2018) described the main characteristics of the product and evaluated it at different time scales. A sea level budget and comparison with other data sets (sea level products from other institutions, global and regional models, in situ data) was also performed with results matching well the in situ reference (Ablain et al., 2017; Legeais et al., 2018).

2.3. Steric Sea Level Data: The ISAS Product

The simulated steric sea level variability will be assessed against the in situ Analysis System (ISAS) data set that gathers all in situ measurements especially Argo profiles from January 2002 to December 2015 (Kolodziejczyk et al., 2017). The profiles are interpolated on a regular grid with a 0.5° resolution at the equator getting finer toward high latitudes (Gaillard et al., 2016). The interpolation is done using the optimal interpolation technique where the interpolated field is obtained from a reference field, coming from climatology or forecast, and an anomaly resulting from the difference between the reference and the measurement at the observation points (Gaillard et al., 2016). Monthly mean temperature and salinity gridded products are provided down to 2,000-m depth.

2.4. Methodology

2.4.1. Sea Level

Simulated sea surface height (SSH) fields from the 50-member OCCIPUT ensemble simulations are considered between 1993 and 2015. Greatbatch (1994) highlighted that Boussinesq models assuming a constant volume cannot properly resolve the GMSL evolution because the steric effect is not taken into account. To account for this in all members, the GMSL (which is the global weighted average) time series is removed at each grid point to obtain monthly sea level anomalies (SLA) relative to their global average. To investigate the interannual variability of regional sea level at each grid point, we first compute successive yearly SLA averages within each member in order to remove the intraannual variability. Then, we use the least-square method to remove the linear trend over 1993–2015 from each of the members of the OCCIPUT ensemble. The resulting fields thus provide an adequate data set to investigate the sea level interannual variability at each grid point over 1993–2015.

SLA corresponds to the sum of their steric anomaly and manometric anomaly components (Equation 1, Gill & Niller, 1973)

$$SLA = \Delta h_{steric} + \Delta h_{manometric}. \tag{1}$$

The steric sea level anomalies Δh_{steric} were computed between 1993 and 2015 within each ensemble member using the monthly temperature and salinity fields, following Equation 2:

$$\Delta h_{steric} = -\int_{H=bottom}^{H=SSH} \frac{\rho'(T,S,p)}{\rho_0} dz, \tag{2}$$

where ρ' is the in situ density anomaly computed as a difference between the sea water density for temperature T, salinity S, and pressure p and a reference density for $T = 0°C$ and $S = 35$ PSU at the same standard level. ρ_0 is set to 1,035 kg m^{-3} (as recommended in Madec, 2016). We applied on steric time series the same yearly averaging and detrending process as described for the SLA time series. The manometric sea level time series were then obtained by subtracting steric sea level from SSH time series (Equation 1), by removing the manometric GMSL time series and by applying the yearly averaging and detrending process.

2.4.2. Ensemble Statistics

The atmospherically forced and chaotic ocean variabilities may be disentangled from ensemble simulations using simple statistics, as presented below. The validity of this classical approach is first assessed as done in

Llovel et al. (2018): we use a Lilliefors test to check whether the ensemble distributions of yearly sea level anomalies, of its steric and manometric components, remain close to Gaussian at every grid point and every year between 1993 and 2015. We found that the percentage of the global ocean area where the Gaussianity of the distribution is rejected at the 95% significance level varies between 4% and 6% for the sea level and its steric component, and between 2% and 8% for the manometric sea level. The ensemble distributions of these yearly fields may thus be considered as Gaussian over most of the Global Ocean, and may be processed as follows.

We followed the method presented in Leroux et al. (2018) to compute the atmospherically forced and chaotic parts of regional sea level interannual variabilities, and of its steric and manometric components. Over-bars are used to indicate the time mean over 1993–2015.

For each sea level component, the ensemble mean $H(t)$ is defined as the average of the 50 members at each point for each year. For each member i, the sea level $h_i(t)$ is then the sum of the ensemble mean $H(t)$ and the chaotic contribution $h'_i(t)$ at each grid point (Equation 3)

$$h_i(t) = H(t) + h'_i(t). \tag{3}$$

The forced variability σ_{forced} is then given by the temporal standard deviation of the ensemble mean of each variable at each grid point (Equation 4)

$$\sigma_{forced} = \sqrt{\frac{1}{T-1} \sum_{t=1}^{T} \left(H(t) - \overline{H(t)} \right)^2}. \tag{4}$$

For each year, we also compute the ensemble variance of each sea level component ($\epsilon_{chaotic}$, Equation 5)

$$\epsilon_{chaotic}^2 = \frac{1}{N-1} \sum_{i=1}^{N} h'_i(t)^2, \tag{5}$$

where $N = 50$ is the number of members. The chaotic variability ($\sigma_{chaotic}$, Equation 6) is then given by their temporal average

$$\sigma_{chaotic} = \sqrt{\overline{\epsilon_{chaotic}^2}}. \tag{6}$$

The total variance σ_{tot}^2 is defined as the ensemble average of the temporal variance of $h_i(t)$ within each member

$$\sigma_{tot}^2 = \frac{1}{N} \sum_{i=1}^{N} \left[\frac{1}{T-1} \sum_{t=1}^{T} \left(h_i(t) - \overline{h_i(t)} \right)^2 \right]. \tag{7}$$

As shown in Leroux et al. (2018), the total, chaotic and forced variabilities are linked by the following equations:

$$\sigma_{tot}^2 = \sigma_{chaotic}^2 + \sigma_{forced}^2. \tag{8}$$

As in Sérazin et al. (2015), we also evaluate the ratio R, which quantifies the contribution of the chaotic variance (numerator) in the total variance (denominator) of SLA and of its components

$$R = \frac{\sigma_{chaotic}^2}{\sigma_{tot}^2}. \tag{9}$$

In the following, we will estimate the percentage of the global ocean area where the chaotic contribution to the total sea-level variance cannot be neglected. Although this threshold is somewhat arbitrary, we propose to include in this category the regions where the R ratio exceeds 20%.
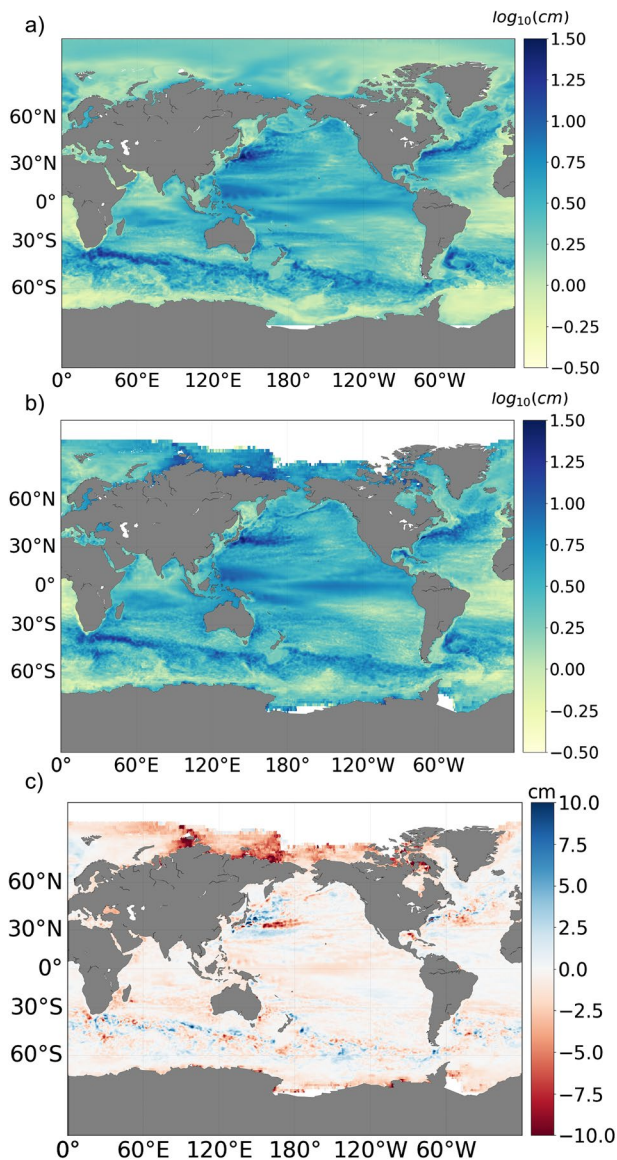
Figure 1. Standard deviation of the yearly averaged and detrended sea level anomalies over 1993–2015 for (a) member 1; (b) CCI product. (c) Differences between the model and the observations. Plots are in logarithmic scales, base 10, for panels a and b. All units are cm.

Finally, we introduce the R_{forced} and $R_{chaotic}$ ratios to quantify the contribution of the manometric component in the atmospherically forced (R_{forced}) and in the chaotic ($R_{chaotic}$) interannual sea level sea-level variance

$$R_{forced,manometric} = \frac{\sigma^2_{forced,manometric}}{\sigma^2_{forced}}, \qquad (10)$$

$$R_{chaotic,manometric} = \frac{\sigma^2_{chaotic,manometric}}{\sigma^2_{chaotic}}, \qquad (11)$$

where $\sigma_{forced,\ manometric}$ and $\sigma_{chaotic,\ manometric}$ correspond to the atmospherically forced and chaotic parts of the manometric sea level interannual variability, calculated as described in Equations 4 and 6.

3. Model Assessment

3.1. Sea Level: Model vs. the CCI Product

The regional sea level interannual variability simulated by the model (Figure 1a) is assessed against the CCI product (Figure 1b) by comparing their temporal standard deviations over the altimetry period (1993–2015). The CCI product is compared to a randomly chosen member from the ensemble (member 1), since the 50 members simulate equiprobable realizations of the ocean evolution over this period.

At each grid point, the yearly averaged detrended SLA standard deviation is computed for both products and represented in logarithmic scale. The CCI product exhibits high values in western boundary current systems, in the equatorial band, and in the ACC. We find sea level interannual variability hotspots in the Agulhas current system and Argentinian basin, in the South Indian Ocean, around the Gulf of Mexico, and along the Russian, Somalian, and Indian coasts.

In comparison, member 1 of the ensemble simulation represents quite well the spatial patterns of regional sea level interannual variability, except along the Russian coasts. For both products, the variability is quite weak in the southeastern Pacific (between 10°S and 30°S) and the tropical Atlantic Ocean (from 0°S to 30°S). The differences between the model and the observations are shown in Figure 1c. They are mainly located in regions of intense mesoscale activity: Gulf Stream, Kuroshio, ACC, and along the Russian coasts.

The observational estimate (Figure 1b) shows blue values corresponding to a very large variability at high latitudes. These regions are located at the limits of the altimetry spatial coverage which has a maximum inclination of 98.55° (for SARAL/AltiKa, ERS 1–2, and ENVISAT missions). These regions are also partially ice-covered during some periods of the year leading to gaps in time series which may explain their high interannual variability values. In these regions, observational results must be taken with caution as the presence of ice and the proximity to the coast may bias the interannual sea level estimations. Despite these local discrepancies between observations and member 1, the numerical model shows a good skill in simulating the interannual variability of regional sea level over 1993–2015.
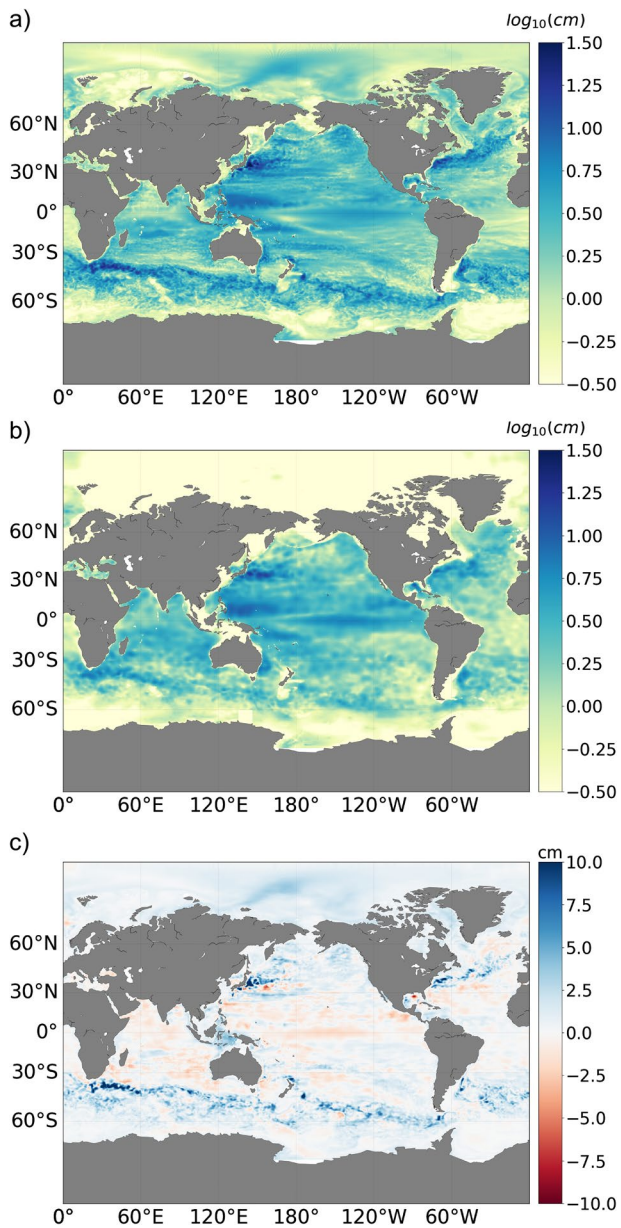
Figure 2. Standard deviation of the yearly averaged and detrended regional steric sea level anomalies over 2005–2015 for (a) member 1; (b) ISAS product. (c) Differences between the model and the observations. Plots are in logarithmic scales, base 10, for panels a and b. All units are cm.

3.2. Steric Sea Level: Model vs. the ISAS Product

The simulated steric sea level interannual variability is now assessed against the ISAS product. We consider the 2005–2015 period instead of 1993–2015 since the Argo array reached a near global coverage in 2005 (especially south of 40°S), with an unprecedented number of salinity profiles. Figure 2 shows the yearly averaged detrended steric sea level standard deviation for member 1 (Figure 2a), for the ISAS product (Figure 2b), and the differences between the model and the observations (Figure 2c). The ISAS product shows high spatial variability patterns in the western boundary current systems, in the Agulhas region, in the equatorial Pacific band, and in the South Indian Ocean. The observed steric interannual variability is weak at high latitudes.

Member 1 shows similar spatial patterns for the steric sea level and SLA variabilities: a strong interannual variability in the entire Pacific Ocean, along the Gulf stream, within the ACC and in the South Indian Ocean. The interannual steric variability in member 1 (Figure 2c) is stronger than observed in the ACC, in the western boundary currents and in the maritime continent region. This could be explained by three main reasons. The ISAS product relies mainly on Argo profiles which are likely to be ejected from the highly turbulent western boundary currents. The ISAS mapping procedure might also yield too smooth fields and underestimate the actual steric sea level interannual variability. There are also less Argo profiles at high latitudes and off southeast Asia, which could explain the differences in these aforementioned regions.

To summarize, the model proves skillful in simulating both the interannual variability of regional sea level over 1993–2015 and the steric sea level component over 2005–2015. We now take advantage of the 50-member ensemble simulations to disentangle the imprints of the atmospherically forced and the chaotic ocean variability on regional sea level interannual variability and its components over 1993–2015.

4. Results

4.1. Regional Sea Level

We first examine the atmospherically forced (Figure 3a) and chaotic (Figure 3b) parts of the simulated regional sea level interannual variability.

The forced variability map (Figure 3a) shows maxima in the equatorial Pacific with three main hotspots: two on both sides of the equator in the west and one along the equator in the east. Trade winds are strong in these specific regions leading to strong interannual variability linked to the natural modes of variability known as El Nino/La Nina events.

Figure 3b exhibits regions of strong chaotic sea level interannual variability especially in the western boundary currents, in the ACC, in the entire Northern Pacific, and in the Indian and Pacific Oceans between 10°S and 30°S. The western boundary currents near Somalia, the Bay of Bengal, and along the eastern Indian coast present large chaotic contributions that are also found by Sérazin et al. (2015) and in Close et al. (2020). On the contrary, the chaotic variability is weak in the equatorial band where the atmospherically forced response is dominant, as well as along the Antarctic coast and north of 65°N. At high latitudes, the model resolution might indeed be too coarse to properly represent the fine-scale nonlinear processes that feed the chaotic ocean variability. Penduff et al. (2019) also pointed out the
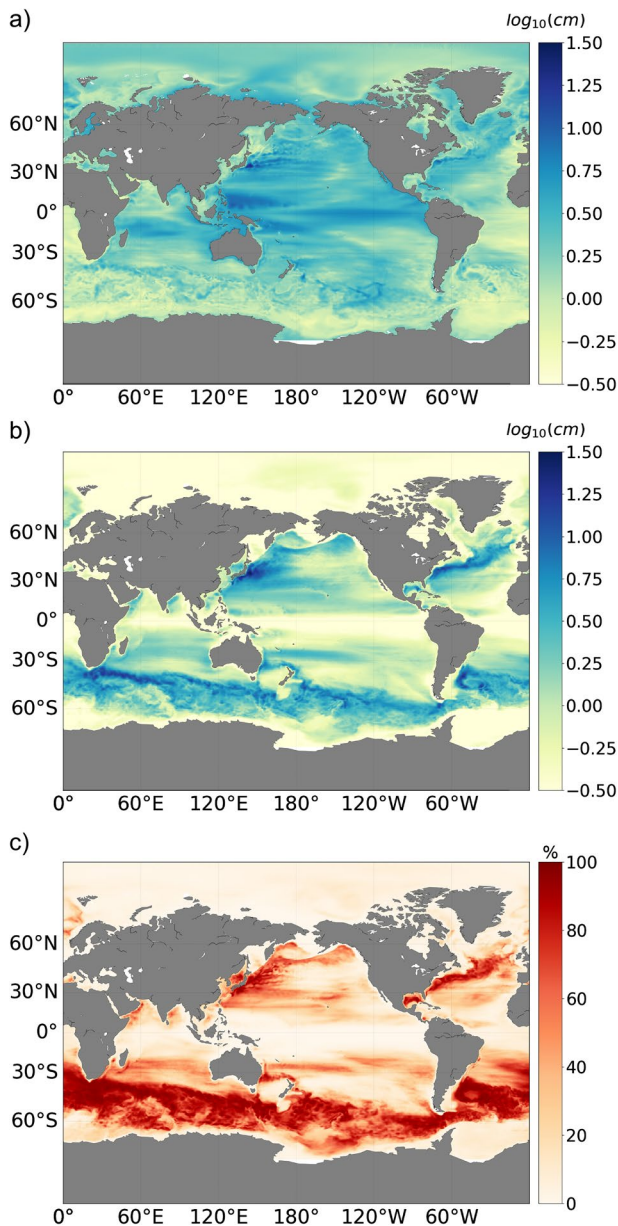
Figure 3. Maps of the atmospherically forced (a) and chaotic (b) interannual variabilities of regional sea level in the OCCIPUT ensemble. The *R* ratio is shown in panel c. Panels a and b are shown with logarithmic scales, base 10. Units are cm in a and b, and percent in c.

decrease of chaotic regional sea level trends in coastal and shallow regions, presumably due to the limited model resolution and because smaller mesoscale processes are likely to have temporal scales shorter than interannual.

The contribution of the chaotic variability to the total interannual sea level variability (*R* ratio) is shown in Figure 3c. It shows that the regional sea level interannual variability is mostly chaotic in the western boundary currents and in the ACC, where there is a strong mesoscale activity. This result is in line with previous analyses of regional sea level variability and trends (Close et al., 2020; Llovel et al., 2018; Penduff et al., 2011; Sérazin et al., 2015). Sérazin et al. (2018) showed that the inverse cascade of kinetic energy can feed the chaotic interannual variability from the mesoscale activity. However, the atmospheric forcing explains most of the variability in the equatorial band.

As mentioned in Section 2, we focus on the regions where the chaotic interannual variability can no longer be considered as negligible. We arbitrarily set this threshold to *R* = 20%; this will be discussed in Section 5. The *R* ratio exceeds 20% over 48% over the global ocean area, denoting the large imprint of chaotic variability. Llovel et al. (2018) showed that regional sea level trends over the same period 1993–2015 cannot be unambiguously attributed to atmospheric forcings over 38% of the global ocean area because of the multidecadal chaotic variability. The *R* ratio reaches large values in strongly eddying current systems: between 60% and 90% in the Kuroshio, 75% and 85% in the Gulf Stream, and above 90% in the ACC. This means that the interannual variability of regional sea level is mostly chaotic in these regions in this 1/4° model simulation. In the equatorial band (10°S–10°N), *R* values do not exceed 7%. These values and their spatial distribution are largely consistent with the results of Penduff et al. (2011) who investigated the contribution of the chaotic variability on regional sea level at interannual time scales over 1993–2004.

4.2. Components of Regional Sea Level Interannual Variability

We now investigate the baroclinic or barotropic origin of the atmospherically forced and chaotic interannual sea level variabilities. For that purpose, we partition the interannual variability of sea level into its steric and manometric components.

Figure 4 presents the atmospherically forced and chaotic parts of the interannual variability of steric sea level computed over the period 1993–2015. Figure 4a shows the atmospherically forced steric sea level interannual variability. The SLA (Figure 3a) and steric (Figure 4a) maps present similar spatial patterns: the main spatial patterns described in Figure 3a (hotspots in the Pacific, western boundary currents) are also found in the steric maps, indicating that the forced sea level variability has a baroclinic origin in many regions. However, Figure 4a shows a weaker forced steric variability at high latitudes and in coastal areas. These results are very similar to those found by Forget and Ponte (2015), who investigated the steric and manometric components of the regional sea level interannual variability over 1993–2010 from the 3°-smoothed outputs of a 1°-simulation based on the MITgcm (Massachusetts Institute of Technology general circulation model). The realism of these authors' data assimilative simulation on this partition appears comparable with ours, which was run without assimilation. However, the patterns in Forget and Ponte (2015) have smaller amplitudes and larger scales as their model is more laminar. They speculate that the strong baroclinic sea level interannual variability at
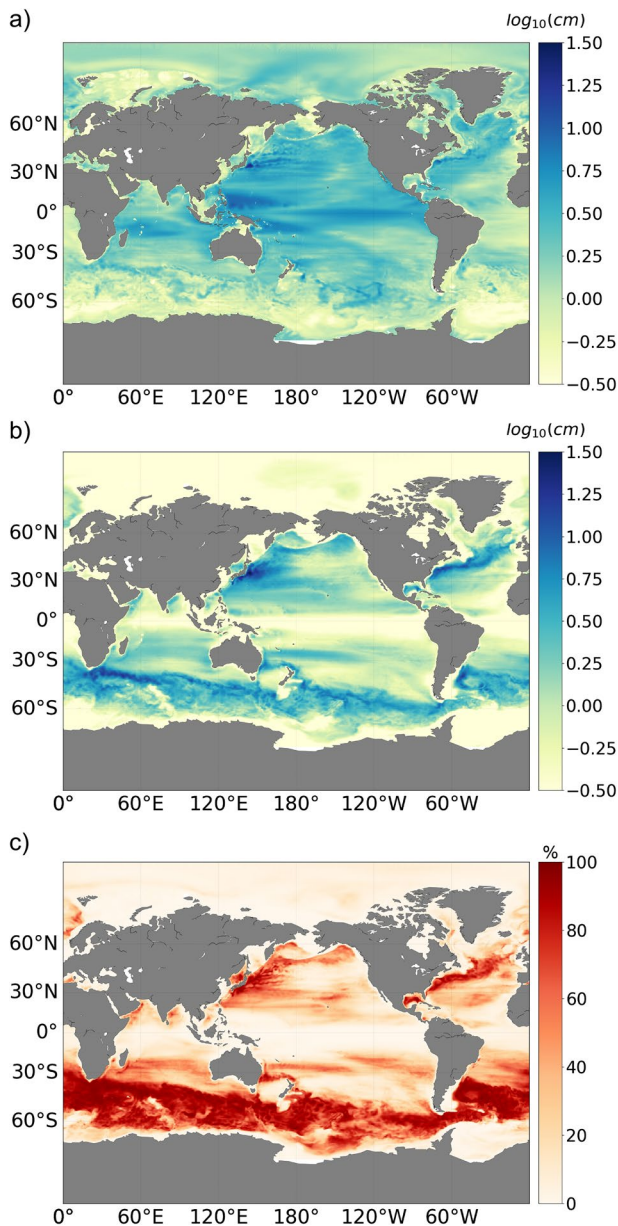
a)

b)

c)

Figure 4. Same as Figure 3 for the steric sea level component.

low latitudes, also visible in Figure 4, is caused by atmospheric forcings and baroclinic waves such as Rossby and Kelvin waves.

As for regional sea level, the steric component exhibits patterns of strong chaotic interannual variability especially in western boundary currents, in the ACC, and in the central Pacific between 0°N and 30°N (Figure 4b). The western boundary currents near Somalia in the Bay of Bengal and along the eastern Indian coast noted previously, therefore, have a steric origin.

The ratio R for the steric sea level interannual variability is shown in Figure 4c. This map presents similar regional structures as those identified for regional sea level (Figure 3c). The interannual steric sea level variability cannot be only attributed to atmospheric forcing in the western boundary currents, in the ACC and along the Somalian and Indian coasts. The steric R ratio exceeds 20% over 48% of the global ocean area. Values of R are almost identical to those reported for SLA: >88% in the ACC, between 60% and 90% in the Kuroshio, and between 75% and 85% in the Gulf Stream. In the equatorial band (10°S–10°N), almost all R values do not exceed 6%, confirming the atmospherically forced origin of steric sea level variability there. These ratios are in the same order of magnitude as for the regional sea level interannual variability ratios.

After investigating the nature of the baroclinic (i.e., steric) component of regional interannual variability, we now focus on the barotropic (i.e., manometric) component over 1993–2015.

Figure 5a shows the atmospherically forced part of the manometric sea level interannual variability. Large values are located in coastal regions such as in the Bering Strait, the Russian coast, the Baltic Sea, and the southeast Asia coast. This confirms that the atmospherically forced regional sea level interannual variability near the coast has a manometric origin. Indeed, in coastal regions, the bathymetry is shallower leading to barotropic responses to the atmospheric variability, which induces water motions throughout the entire water column. In the open ocean, the forced manometric sea level interannual variability is weak except in some parts of the ACC (southeastern Indian and Pacific Oceans, Argentinian basin). These results are in line with Forget and Ponte (2015) who highlight that at high latitudes, the sea level interannual variability has a large manometric component.

Figure 5b depicts the chaotic manometric sea level interannual variability that appears to be weaker than its steric counterpart. However, we find that this chaotic variability reaches large values mainly in the western boundary currents (Gulf Stream, Kuroshio), in the ACC, and in the Argentinian basin (Figure 5b).

The ratio R for the manometric sea level component (Figure 5c) shows that the interannual variability cannot be only attributed to atmospheric variability in the western boundary currents and in the ACC. The manometric sea level R ratio exceeds 20% over 26% of the global ocean area. Compared to its steric counterpart, the manometric sea level R ratio exceeds 20% over a smaller fraction (26%) of the global ocean area.

Figure 6 shows the $R_{forced, manometric}$ (Figure 6a) and $R_{chaotic, manometric}$ (Figure 6b) maps that represent the percentage of the atmospherically forced and chaotic variabilities explained by the manometric sea level component. Both maps exhibit large values in coastal and shallow regions, and in several regions of the Southern Ocean. This highlights the dominance of barotropic processes in these regions for both the atmospherically forced
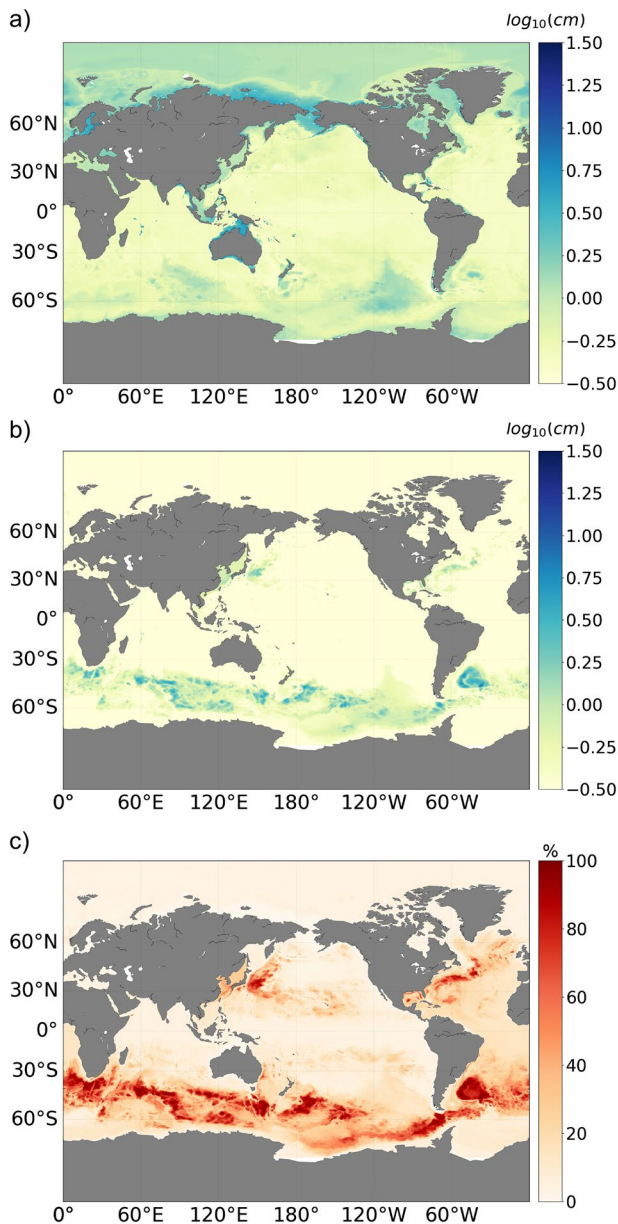
Figure 5. Same as Figure 3 for the manometric sea level component.

and chaotic variabilities. On the other hand, weak values highlight the dominance of baroclinic processes (i.e., steric sea level interannual variability) especially in the tropical and midlatitude parts of the open ocean.

The $R_{forced, \, manometric}$ and $R_{chaotic, \, manometric}$ ratios are mostly greater than 90% in regions shallower than 200 m. The contrast between the open ocean and the coasts is stronger for the chaotic variability (Figure 6b). At low latitudes (<30°), where baroclinic processes are important, the atmospherically forced and chaotic steric sea level component reaches >90%. In the ACC, the barotropic processes explain <7% and 16% of the chaotic and forced variability.

4.3. Zonally Averaged Contributions of Forced and Chaotic Sea Level Interannual Variability

As both the atmospherically forced and chaotic parts of the regional sea level interannual variability present large geographical contrasts, we further investigate their respective contributions by comparing their zonal averages both at global and at basin scales. We focus here on the latitudes and the ocean basins where the chaotic variability is greater than its atmospherically forced counterpart.

Figure 7 exhibits large zonally averaged values of chaotic sea level interannual variability in the ACC (2.5–3 cm) and in the western boundary currents (1.5–1.7 cm) latitude bands. The atmospherically forced variability is equivalent to the chaotic variability at the latitudes of the western boundary currents. The atmospherically forced variability (1–2 cm) is much smaller than its chaotic counterpart in the latitudinal range of the ACC. We find similar results for the zonally averaged steric sea level interannual variability, confirming the large contribution of baroclinic processes at the global scale. The zonally averaged atmospherically forced variability of the manometric sea level is always larger than its chaotic counterpart except within the ACC where both variabilities compete with each other. In the equatorial band, the atmospherically forced variability dominates the zonally averaged interannual variability of sea level and of its steric component. Figure 7 thus confirms the conclusions inferred from the maps shown in Figures 3–5: the steric component explains a large part of the atmospherically forced and chaotic regional sea level interannual variability.

We now extend this analysis to each ocean basin taken individually. Figure 8 shows these different contributions in the Pacific (a, b, c), the Atlantic (d, e, f), and the Indian (g, h, i) Oceans.

The zonally averaged atmospherically forced sea level interannual variability is greater than its chaotic counterpart in the three basins, except at the latitudes of the western boundary currents and of the northern ACC (around 40°N and 40°S). The same holds for the steric sea level component: the zonally averaged atmospherically forced sea level interannual variability has a steric origin almost everywhere, except north of 45°N in the Pacific Ocean where the manometric sea level component becomes larger. We also note, in addition to the conclusions inferred from Figures 3 and 4, that the forced variability of the sea level and its steric component is stronger in the equatorial band in the Pacific and Indian basin than in the Atlantic Ocean. With the exception of the ACC region, the zonally averaged chaotic interannual variabilities of sea level and of its components happen to exceed their atmospherically forced counterparts mostly in the Atlantic Ocean. The variability of manometric sea level is mostly driven by the atmosphere, except in around 40°S–50°S.

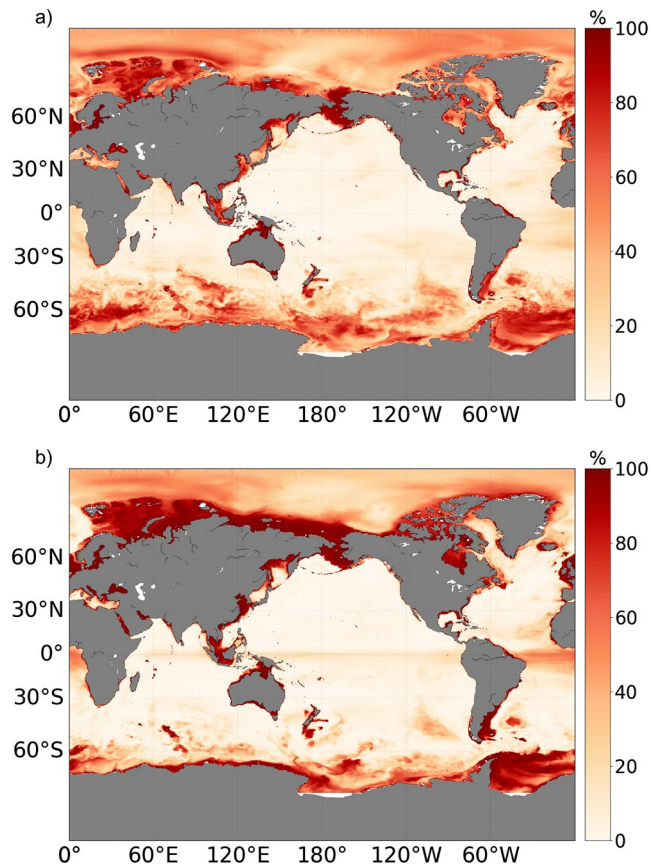**Figure 6.** Percentage of the (a) atmospherically forced and (b) chaotic interannual sea level variability explained by the barotropic (i.e., manometric) component. Units are percent.

5. Conclusions and Discussion

In this study, we used a 50-member ocean/sea-ice ensemble simulation to disentangle over 1993–2015 the atmospherically forced and chaotic parts of the interannual variability of regional sea level, and of its steric and manometric components.

We first showed that this NEMO simulation skillfully represents the observed interannual variability of regional sea level (over 1993–2015), as well as of its steric components (over 2005–2015). We then took advantage of the simulation's ensemble dimension to evaluate the contributions of the atmospherically forced and chaotic intrinsic ocean variability in the variability of sea level and of its two components.

We find large values of atmospherically forced interannual variability of regional sea level at low latitudes and in the western boundary currents, especially in the Gulf Stream and the Kuroshio. Chaotic sea level interannual variability reaches its maxima in the western boundary currents and in the ACC. The contribution of chaotic variability to the sea level interannual variability exceeds 20% over 48% of the global ocean area; in other words, this source of random sea level interannual fluctuations is substantial and cannot be neglected over about half of the global ocean area. The sea level interannual chaotic variability reaches its largest relative contribution in the ACC ($R \sim 90\%$), in the Gulf Stream ($R \sim 80\%$), and in the Kuroshio ($R \sim 60$–90%).

The amplitude, distribution, and relative contribution of the sea level chaotic interannual variability diagnosed from the OCCIPUT ensemble are consistent with those estimated from a pair of global ocean simulations (one driven by a repeated seasonal cycle, one driven by a fully variable reanalyzed forcing) by Penduff et al. (2011) at the same 1/4° resolution. Sérazin et al. (2015), however, showed that the amplitude of chaotic sea level interannual variability is smaller at a model resolution of 1/4° than at a model resolution of 1/12°, suggesting that our estimates of the chaotic contribution to sea level variability may be underestimated.

Sérazin et al. (2017) showed that the interannual variability of OHC over 1980–2010 is also dominantly chaotic in the aforementioned regions (ACC and western boundary currents). Interestingly, the OHC chaotic variability map presents similar hotspots for both the regional sea level trends (Llovel et al., 2018) and the regional sea level interannual variability (this study), suggesting the multivariate and multiscale nature of the chaotic ocean variability.

Forget and Ponte (2015) decomposed the regional sea level interannual variability over 1993–2011 into atmospherically forced and chaotic parts. They hypothesize that the atmospheric variability impacts sea level fluctuations over large scales (>3° × 3°). They consider that sea level fluctuations at scales smaller than 3° were chaotic. This is a strong hypothesis that we challenge in the present study. Our results show that considering an ensemble simulation allows to disentangle properly the atmospherically forced and chaotic signals at all spatial scales without such an assumption.

The second scientific question addressed in this paper concerns the barotropic or baroclinic origin of the regional sea level interannual variability. We found that the atmospherically forced and chaotic parts of regional sea level interannual variability mostly have a steric origin, except in coastal and shallow areas where these variabilities are driven by barotropic processes (Figure 6). This result is consistent with Penduff et al. (2019), and with Landerer et al. (2017) who showed that barotropic gravity waves redistribute toward the shelves the volume anomalies created by steric changes in open ocean. The chaotic-to-total interannual variability ratio exceeds 20% over 48% of the global ocean area for the steric component, with
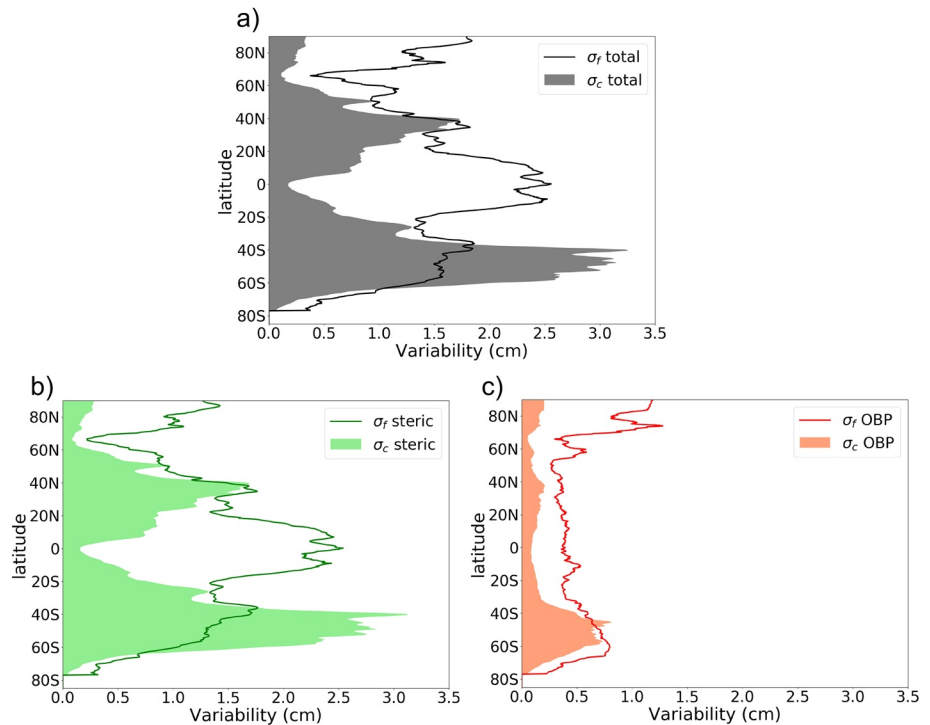
Figure 7. Zonally averaged atmospherically forced (solid lines) and chaotic (filled areas) interannual variabilities of (a) sea level anomalies, (b) steric, and (c) manometric sea level anomalies over the global ocean. Units are cm.

values reaching 88% in the ACC, 80% in the Gulf stream and between 60% and 90% in the Kuroshio (Figure 4c). The chaotic contribution is less important for the manometric sea level with an R ratio exceeding 20% over 26% of the global ocean area. Our results are in line with those in Forget and Ponte (2015), who showed that sea level variabilities at periods between 3 months and 3 years are mainly barotropic at high latitudes and baroclinic at low latitudes. Here, we go further by quantifying the contribution of barotropic processes to the chaotic and atmospherically forced variabilities, with an alternative approach.

Penduff et al. (2019) investigated the steric and manometric contributions of regional sea level trends in the global and coastal ocean over 1993–2015. They found that forced manometric trends are 4–10 times stronger in coastal and shallow regions than in the open ocean. One of their main results is that sea level trends cannot be unambiguously attributed to atmospheric forcings over 17% (30% for the manometric contribution) of the coastal part of the global ocean area. Our results complement the latter study and show that the steric component explains most of the sea level interannual variability in the open ocean, whereas the manometric component explains most of it in the coastal and shallow regions (for both the atmospherically forced and chaotic variabilities). The chaotic variability in the ACC is mainly baroclinic with a barotropic component further south, near the Antarctic coast.

This paper also focused on the zonally averaged contributions of the atmospherically forced and chaotic variability and their variations from one ocean basin to the other. These results confirm the mostly steric origin of interannual sea level variability in all ocean basins, except at high latitudes where the barotropic component becomes more important. In each basin, the atmospherically forced contribution is always greater than the chaotic contribution except in the strongest eddy-active currents: around 40°S in the ACC and 40°N in western boundary current extensions (Gulf Stream and Kuroshio). At these latitudes, the situation depends on the basin: the chaotic contribution exceeds the forced one within the ACC in the three oceans but it becomes much stronger than the latter in the Atlantic Ocean's western boundary currents.

The chaotic interannual variability of sea level and its steric component is strongly dominated by its forced counterpart in the equatorial band, except in the Atlantic Ocean where the latter is smaller. These differenc-
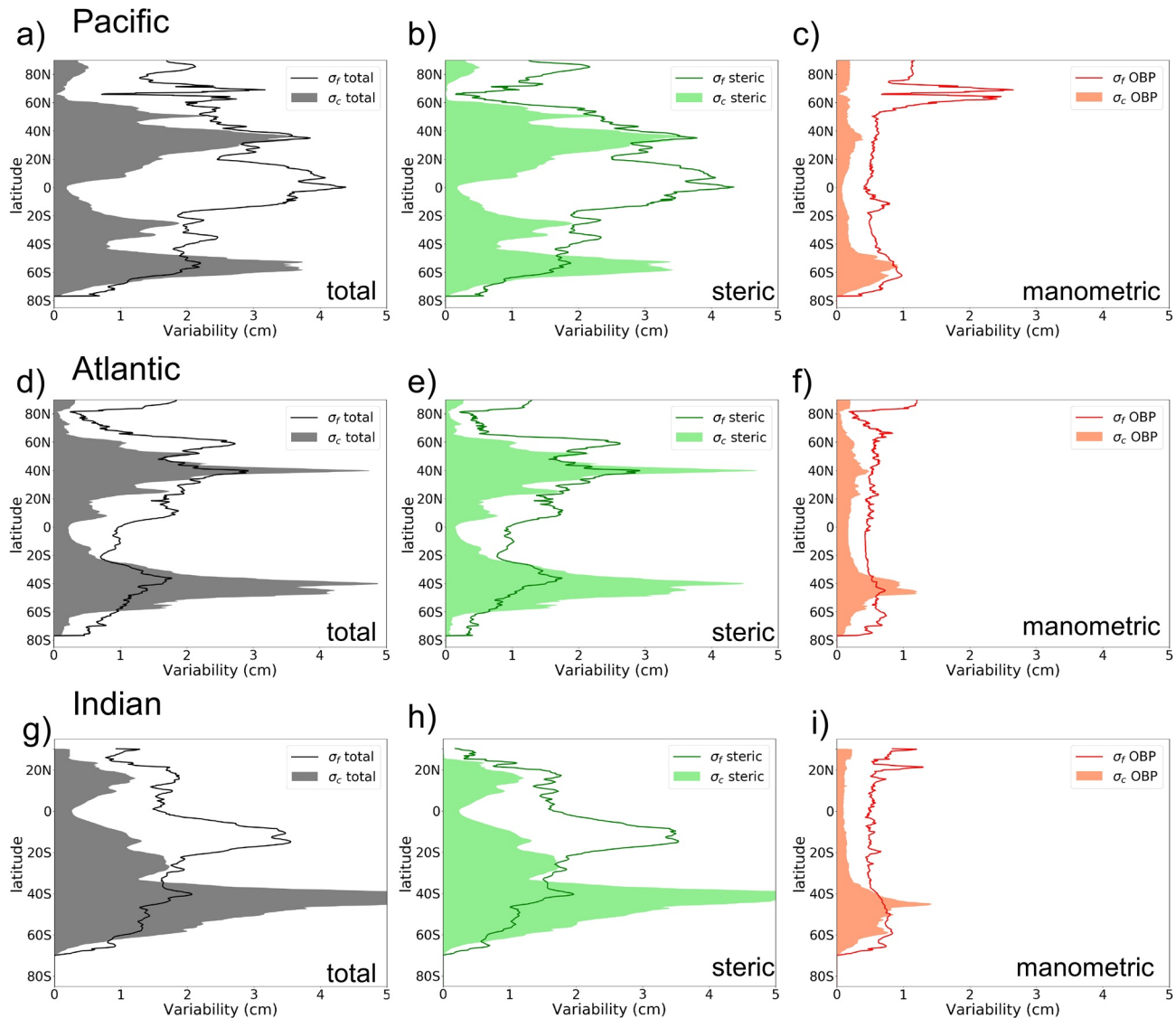
Figure 8. Zonal averages of the atmospherically forced (σ_f, solid lines) and the chaotic (σ_c, filled areas) variabilities of the total (in black, a, d, g), steric (in green, b, e, h), and manometric (in red, c, f, i) sea level in the Pacific (a, b, c), the Atlantic (d, e, f), and the Indian (g, h, i) Oceans. Units are in cm.

es are likely linked to the dominant modes of atmospheric variability which mostly impact the equatorial band in the Pacific Ocean (La Nina/El Nino) and the Indian Ocean (Indian Ocean Dipole), while the North Atlantic Oscillation impacts regions located further north in the Atlantic Ocean.

The present study enables us to go one step further to quantify to what extent the chaotic interannual variability explains the total interannual variability of regional sea level and its components. We found that over 48%, 48% and 26% of the global ocean area, the relative part of the chaotic interannual variability (R ratio) exceeds 20% for the sea level, steric, and manometric components, respectively. The interannual chaotic variability is thus important and it raises new questions on its detection in observations, its disentangling from the atmospherically forced interannual variability and its characterization (as a function of depth or the time period considered).

Investigating these questions could help us take the chaotic variability into account in the interpretation of oceanic observations. However, the reader must not forget that these figures depend on the limit we chose for R. R values greater than 50%, which means a chaotic contribution more important than the forced

contribution, is found over 22%, 23%, and 8% of the global ocean area for the sea level and its steric and manometric components, respectively.

Despite their consistency with various previous studies, our results may be sensitive to the choice of the numerical model; it would be interesting to apply the same analysis to other ensemble simulations, at different resolutions or driven by different forcing fields. Previous studies showed that the chaotic sea level interannual variability simulated at 1/4° resolution strongly drops when the model resolution is coarser (i.e., 2°; Penduff et al., 2011), and further increases when the resolution is finer (i.e., 1/12°; Sérazin et al., 2015). Although the computational cost of a 1/12° equivalent of the OCCIPUT large ensemble may be prohibitive by today's standards, it is clear that it could yield great progress for studies of this kind, in particular, where the mesoscale activity is underestimated at 1/4° (e.g., at high latitudes or in shallow regions). Regional ensembles at increased resolution, potentially driven by OCCIPUT outputs at their boundaries, could help us to investigate such areas where climate change has large impacts, for an affordable computational cost.

Data Availability Statement

The CCI product is freely available at http://www.esa-sealevel-cci.org. ISAS temperature and salinity products were produced and distributed by the French Service National d'Observation Argo at LOPS (https://www.seanoe.org/data/00412/52367/). To reproduce the presented results, the model code (NEMO3.5 version) can be downloaded at http://forge.ipsl.jussieu.fr/nemo.wiki/Users. The DFS5.2 forcings are available at http://servdap.legi.grenoble-inp.fr/meom/DFS5.2/. The ensemble strategy is described in Bessières et al. (2017). Finally, we thank the anonymous reviewers for their constructive comments, which helped to improve the quality of the paper.

References

Ablain, M., Legeais, J. F., Prandi, P., Marcos, M., Fenoglio-Marc, L., Dieng, H. B., et al. (2017). Satellite altimetry-based sea level at global and regional scales. *Surveys in Geophysics*, *38*(1), 7–31. https://doi.org/10.1007/s10712-016-9389-8

Arbic, B. K., Müller, M., Richman, J. G., Shriver, J. F., Morten, A. J., Scott, R. B., et al. (2014). Geostrophic turbulence in the frequency-wavenumber domain: Eddy-driven low-frequency variability. *Journal of Physical Oceanography*, *44*, 2050–2069. https://doi.org/10.1175/JPO-D-13-054.1

Bamber, J. L., & Dawson, G. J. (2020). Complex evolving patterns of mass loss from Antarctica's largest glacier. *Nature Geoscience*, *13*(2), 127–131. https://doi.org/10.1038/s41561-019-0527-z

Bessières, L., Leroux, S., Brankart, J.-M., Molines, J.-M., Moine, M.-P., Bouttier, P.-A., et al. (2017). Development of a probabilistic ocean modelling system based on NEMO 3.5: Application at eddying resolution. *Geoscientific Model Development*, *10*(3), 1091–1106. https://doi.org/10.5194/gmd-10-1091-2017

Brankart, J.-M. (2013). Impact of uncertainties in the horizontal density gradient upon low resolution global ocean modelling. *Ocean Modelling*, *66*, 64–76. https://doi.org/10.1016/j.ocemod.2013.02.004

Cazenave, A., & Llovel, W. (2010). Contemporary sea level rise. *Annual Review of Marine Science*, *2*(1), 145–173. https://doi.org/10.1146/annurev-marine-120308-081105

Church, J. A., Clark, P. U., Cazenave, A., Gregory, J. M., Jevrejeva, S., Levermann, A., et al. (2013). Sea level change. In T. F. Stocker, D. Qin, G.-K. Plattner, M. Tignor, S. K. Allen, J. Boschung, et al. (Eds.), *Climate change 2013: The physical science basis. Contribution of working Group I to the Fifth Assessment Report of the Intergovernmental Panel on Climate Change*. Cambridge, UK and NY, NY: Cambridge University Press.

Close, S., Penduff, T., Speich, S., & Molines, J.-M. (2020). A means of estimating the intrinsic and atmospherically-forced contributions to sea surface height variability applied to altimetric observations. *Progress in Oceanography*, *184*, 102314. https://doi.org/10.1016/j.pocean.2020.102314

Dussin, R., Barnier, B., Brodeau, L., & Molines, J. M. (2016). *The making of Drakkar forcing set DFS5. DRAKKAR/MyOcean report 01-04-16*. Grenoble, France: IGE.

Forget, G., & Ponte, R. M. (2015). The partition of regional sea level variability. *Progress in Oceanography*, *137*, 173–195. https://doi.org/10.1016/j.pocean.2015.06.002

Gaillard, F., Reynaud, T., Thierry, V., Kolodziejczyk, N., & von Schuckmann, K. (2016). In situ-based reanalysis of the global ocean temperature and salinity with ISAS: Variability of the heat content and steric height. *Journal of Climate*, *29*(4), 1305–1323. https://doi.org/10.1175/jcli-d-15-0028.1

Gill, A. E., & Niller, P. P. (1973). The theory of the seasonal variability in the ocean. *Deep Sea Research and Oceanographic Abstracts*, *20*(2), 141–177. https://doi.org/10.1016/0011-7471(73)90049-1

Greatbatch, R. J. (1994). A note on the representation of steric sea level in models that conserve volume rather than mass. *Journal of Geophysical Research*, *99*(C6), 12767–12771. https://doi.org/10.1029/94JC00847

Gregory, J. M., Andrews, T., Ceppi, P., Mauritsen, T., & Webb, M. J. (2019). How accurately can the climate sensitivity to CO_2 be estimated from historical climate change? *Climate Dynamics*, *54*(1–2), 129–157. https://doi.org/10.1007/s00382-019-04991-y

Kolodziejczyk, N., Prigent-Mazella, A., & Gaillard, F. (2017). *ISAS-15 temperature and salinity gridded fields [Data set]*. SEANOE. https://doi.org/10.17882/52367

Landerer, F. W., Jungclaus, J. H., & Marotzke, J. (2017). Ocean bottom pressure changes lead to a decreasing length-of-day in a warming climate. *Geophysical Research Letters*, *34*, L06307. https://doi.org/10.1029/2006GL029106

Legeais, J.-F., Ablain, M., Zawadzki, L., Zuo, H., Johannessen, J. A., Scharffenberg, M. G., et al. (2018). An improved and homogeneous altimeter sea level record from the ESA climate change initiative. *Earth System Science Data*, *10*(1), 281–301. https://doi.org/10.5194/essd-10-281-2018

Leroux, S., Penduff, T., Bessières, L., Molines, J.-M., Brankart, J.-M., Sérazin, G., et al. (2018). Intrinsic and atmospherically forced variability of the AMOC: Insights from a large-ensemble ocean hindcast. *Journal of Climate*, *31*(3), 1183–1203. https://doi.org/10.1175/jcli-d-17-0168.1

Llovel, W., & Lee, T. (2015). Importance and origin of halosteric contribution to sea level change in the southeast Indian Ocean during 2005-2013. *Geophysical Research Letters*, *42*, 1148–1157. https://doi.org/10.1002/2014GL062611

Llovel, W., Penduff, T., Meyssignac, B., Molines, J.-M., Terray, L., Bessières, L., & Barnier, B. (2018). Contributions of atmospheric forcing and chaotic ocean variability to regional sea level trends over 1993–2015. *Geophysical Research Letters*, *45*(24), 13405–13413. https://doi.org/10.1029/2018GL080838

Llovel, W., Purkey, S., Meyssignac, B., Blazquez, A., Kolodziejczyk, N., & Bamber, J. (2019). Global ocean freshening, ocean mass increase and global mean sea level rise over 2005–2015. *Scientific Reports*, *9*(1), 17717.

Madec, G. (2008). *NEMO Ocean Engine. Note du Pole de modélisation*. Institut Pierre-Simon Laplace (IPSL).

Madec, G. (2016). *NEMO Ocean Engine*. Institut Pierre-Simon Laplace (IPSL). Retrieved from https://www.nemo-ocean.eu/doc

Nerem, R. S., Beckley, B. D., Fasullo, J. T., Hamlington, B. D., Masters, D., & Mitchum, G. T. (2018). Climate-change–driven accelerated sea-level rise detected in the altimeter era. *Proceedings of the National Academy of Sciences of the United States of America*, *115*(9), 2022–2025. https://doi.org/10.1073/pnas.1717312115

Neumann, B., Vafeidis, A. T., Zimmermann, J., & Nicholls, R. J. (2015). Future coastal population growth and exposure to sea-level rise and coastal flooding—A global assessment. *PLoS One*, *10*(3), e0118571. https://doi.org/10.1371/journal.pone.0118571

Penduff, T., Juza, M., Barnier, B., Zika, J., Dewar, W. K., Treguier, A.-M., et al. (2011). Sea level expression of intrinsic and forced ocean variabilities at interannual time scales. *Journal of Climate*, *24*(21), 5652–5670. https://doi.org/10.1175/JCLI-D-11-00077.1

Penduff, T., Llovel, W., Close, S., Garcia-Gomez, I., & Leroux, S. (2019). Trends of coastal sea level between 1993 and 2015: Imprints of atmospheric forcing and oceanic chaos. *Surveys in Geophysics*, *40*, 1543–1562. https://doi.org/10.1007/s10712-019-09571-7

Permanent Service for Mean Sea Level (PSMSL). (2020). *Tide gauge data*. Retrieved from http://www.psmsl.org/data/obtaining

Quartly, G. D., Legeais, J.-F., Ablain, M., Zawadzki, L., Fernandes, M. J., Rudenko, S., et al. (2017). A new phase in the production of quality-controlled sea level data. *Earth System Science Data*, *9*(2), 557–572. https://doi.org/10.5194/essd-9-557-2017

Rietbroek, R., Brunnabend, S.-E., Kusche, J., Schröter, J., & Dahle, C. (2016). Revisiting the contemporary sea-level budget on global and regional scales. *Proceedings of the National Academy of Sciences of the United States of America*, *113*(6), 1504–1509. https://doi.org/10.1073/pnas.1519132113

Sérazin, G., Jaymond, A., Leroux, S., Penduff, T., Bessières, L., Llovel, W., et al. (2017). A global probabilistic study of the ocean heat content low-frequency variability: Atmospheric forcing versus oceanic chaos. *Geophysical Research Letters*, *44*, 5580–5589. https://doi.org/10.1002/2017GL073026

Sérazin, G., Meyssignac, B., Penduff, T., Terray, L., Barnier, B., & Molines, J.-M. (2016). Quantifying uncertainties on regional sea level change induced by multidecadal intrinsic oceanic variability. *Geophysical Research Letters*, *43*, 8151–8159. https://doi.org/10.1002/2016GL069273

Sérazin, G., Penduff, T., Barnier, B., Molines, J.-M., Arbic, B. K., Müller, M., & Terray, L. (2018). Inverse cascades of kinetic energy as a source of intrinsic variability: A global OGCM study. *Journal of Physical Oceanography*, *48*(6), 1385–1408. https://doi.org/10.1175/JPO-D-17-0136.1

Sérazin, G., Penduff, T., Grégorio, S., Barnier, B., Molines, J.-M., & Terray, L. (2015). Intrinsic variability of sea level from global ocean simulations: Spatiotemporal scales. *Journal of Climate*, *28*(10), 4279–4292. https://doi.org/10.1175/JCLI-D-14-00554.1

Stammer, D., Cazenave, A., Ponte, R. M., & Tamisiea, M. E. (2013). Causes for contemporary regional sea level changes. *Annual Review of Marine Science*, *5*(1), 21–46. https://doi.org/10.1146/annurev-marine-121211-172406

WCRP Global Sea Level Budget Group. (2018). Global sea-level budget 1993–present. *Earth System Science Data*, *10*, 1551–1590. https://doi.org/10.5194/essd-10-1551-2018

Willis, J. K., Chambers, D. P., & Nerem, R. S. (2008). Assessing the globally averaged sea level budget on seasonal to interannual timescales. *Journal of Geophysical Research*, *113*, C06015. https://doi.org/10.1029/2007JC004517